ELEMENTA
Science of the Anthropocene

Lukovich, JV, et al. 2021. Simulated impacts of relative climate change and river discharge regulation on sea ice and oceanographic conditions in the Hudson Bay Complex. *Elem Sci Anth*, 9: 1. DOI: https://doi.org/10.1525/elementa.2020.00127

RESEARCH ARTICLE

Simulated impacts of relative climate change and river discharge regulation on sea ice and oceanographic conditions in the Hudson Bay Complex

Jennifer V. Lukovich[1,*], Shabnam Jafarikhasragh[1], Paul G. Myers[2], Natasha A. Ridenour[2], Laura Castro de la Guardia[1], Xianmin Hu[2], Nathan Grivault[2], Juliana Marson[1,2], Clark Pennelly[2], Julienne C. Stroeve[1,3,4], Kevin Sydor[5], Karen Wong[5], T. A. Stadnyk[6], and D. G. Barber[1]

In this analysis, we examine relative contributions from climate change and river discharge regulation to changes in marine conditions in the Hudson Bay Complex using a subset of five atmospheric forcing scenarios from the Coupled Model Intercomparison Project Phase 5 (CMIP5), river discharge data from the Hydrological Predictions for the Environment (HYPE) model, both naturalized (without anthropogenic intervention) and regulated (anthropogenically controlled through diversions, dams, reservoirs), and output from the Nucleus for European Modeling of the Ocean Ice-Ocean model for the 1981–2070 time frame. Investigated in particular are spatiotemporal changes in sea surface temperature, sea ice concentration and thickness, and zonal and meridional sea ice drift in response to (i) climate change through comparison of historical (1981–2010) and future (2021–2050 and 2041–2070) simulations, (ii) regulation through comparison of historical (1981–2010) naturalized and regulated simulations, and (iii) climate change and regulation combined through comparison of future (2021–2050 and 2041–2070) naturalized and regulated simulations. Also investigated is use of the diagnostic known as e-folding time spatial distribution to monitor changes in persistence in these variables in response to changing climate and regulation impacts in the Hudson Bay Complex. Results from this analysis highlight bay-wide and regional reductions in sea ice concentration and thickness in southwest and northeast Hudson Bay in response to a changing climate, and east-west asymmetry in sea ice drift response in support of past studies. Regulation is also shown to amplify or suppress the climate change signal. Specifically, regulation amplifies sea surface temperatures from April to August, suppresses sea ice loss by approximately 30% in March, contributes to enhanced sea ice drift speed by approximately 30%, and reduces meridional circulation by approximately 20% in January due to enhanced zonal drift. Results further suggest that the offshore impacts of regulation are amplified in a changing climate.

Keywords: Climate change, Regulation, Hudson Bay Complex, Sea ice, Oceanographic, Simulations

1. Introduction

In this study, we examined simulated climate change and river discharge regulation and their combined impact on marine conditions in Hudson Bay (HB) as a contribution to BaySys, a collaborative project between Manitoba Hydro, the University of Manitoba, the University of Alberta, and Ouranos. Climate change in this study refers to anthropogenic or human-induced change due to greenhouse gas emissions, air pollutant emissions, and land use (Intergovernmental Panel on Climate Change, 2014), while river regulation refers to anthropogenic or human-induced change due to interventions such as dams, reservoirs, and diversions. Specifically, we characterize relative contributions from climate change and river regulation to changes

[1] Centre for Earth Observation Science, University of Manitoba, Winnipeg, MB, Canada
[2] Department of Earth and Atmospheric Sciences, University of Alberta, Edmonton, AB, Canada
[3] Centre for Polar Observation and Modelling, Earth Sciences, University College London, London, UK
[4] National Snow and Ice Data Center, University of Colorado, Boulder, CO, USA
[5] Manitoba Hydro, Winnipeg, MB, Canada
[6] Department of Geography, University of Calgary, Calgary, AB, Canada

* Corresponding author:
Email: jennifer.lukovich@umanitoba.ca

in marine conditions in HB. In the following, we refer to river discharge regulation as "regulation."

Climate change impacts on Arctic sea ice and sea surface temperatures (SSTs) are evidenced in the correspondence between increasing temperatures, associated with global CO_2 increases, and sea ice decline, as demonstrated in Mahlstein and Knutti (2012), Stroeve and Notz (2015), and Notz and Stroeve (2016). Within the Hudson Bay Complex (HBC), future warming trends have been estimated under various greenhouse gas emission scenarios, with mean multimodel ensemble trends of 0.22 ± 0.08°C per decade for representative concentration pathway RCP4.5, and 0.31 ± 0.07°C per decade for RCP8.5 during the 2012–2064 time frame (Lavoie et al., 2013). Difference maps show temperature changes ranging from 1.6 ± 0.6°C in northwest and 4.8 ± 1°C in southeast HB for RCP8.5 emissions scenarios for 2046–2065 versus 1986–2005 (Steiner et al., 2015). Seasonal difference maps show enhanced warming in southeastern HB in summer and fall (Joly et al., 2011).

In response to the projected warming, studies have shown an 11.6% and 15.6% decrease in mean sea ice concentration (SIC) averaged over the entire HBC for the RCP4.5 and RCP8.5 emissions scenarios, respectively, based on comparison of the 2046–2065 and 1986–2005 time frames (Steiner et al., 2015), and an approximate month-long increase in the ice-free season, as demonstrated by freeze-up (breakup) dates shown to occur 25 (22) days later (earlier) based on comparison of the 2041–2070 and 1961–1990 time frames (Joly et al., 2011). Furthermore, sea ice area was shown in their study to decrease in November and December, and from May to June under the influence of a changing climate, while sea ice volume decreased throughout winter (January–April) due to a sustained decrease in ice thickness, with values ranging from approximately 20% and 60% fraction reduction in sea ice thickness (SIT) in northwest and southeast HB, respectively. This northwest/southeast asymmetry in sea ice conditions is reflected in studies of recent spatial/regional variations in SICs (Hochheim and Barber, 2010), thickness (Gagnon and Gough, 2006; Landy et al., 2017), and circulation (Kirillov et al., 2020).

Past studies have explored regulation impacts on river discharge trends, as well as surface temperature and sea ice conditions in HB (Prinsenberg, 1980, 1983; Anctil and Couture, 1994; Ingram and Prinsenberg, 1998; Déry et al., 2011; Déry et al., 2016). Anthropogenic influence on river discharge, or regulation, occurs in the form of irrigation withdrawals, diversions, dams, and reservoirs and influences neighboring surface temperature and sea ice conditions through a change in seasonality in river discharge, and in particular an increase (decrease) in flow rates in winter (summer). The southern segment of HB is influenced by hydroelectric development, while approximately 45% of HB river discharge is regulated (Déry et al., 2018). In the western HB in 1976, 75% (by volume, on average) of the Churchill River at the Missi Falls control structure was diverted into the Nelson River, resulting in a 40% increase in flow (Déry et al., 2011). In the eastern HB in 1980, 80% of the Eastmain River (by volume) was diverted to the La Grande Rivière, resulting in an approximate doubling of its discharge rate. Higher flow rates in winter associated with regulation encourage sea ice formation due to freshening of surface waters (Prinsenberg, 1983; Ingram and Prinsenberg, 1998; Saucier, 2004) and, because river plume area is proportional to discharge (Ingram and Larouche, 1987), the extension of under-ice river plumes (LeBlond et al., 1996; Whittaker, 2006). Through the use of a one-dimensional mixed-layer model, Prinsenberg (1983) showed that regulation encourages early formation of the pycnocline in spring, which lowers the temperature and salinity and which, by isolating near-surface waters from warmer waters at depth combined with surface freezing, stimulates enhanced ice formation. Previous studies have also demonstrated that because the magnitude of density-driven currents is related to the runoff rate, hydroelectric development that increases winter runoff will also increase winter circulation (Prinsenberg, 1991).

Also of interest are the relative and combined impacts of climate change and river discharge regulation on ice and oceanographic conditions. Previous studies have explored the relative impacts of climate change and regulation in Sweden (Arheimer et al., 2017), showing the dominant role that regulation can play in snow-fed rivers on flow regimes, as well as spatial variability. The role of regulation in formulating adaptation strategies was also considered. Lee et al. (2016) evaluated climate impacts on regulation decisions from the perspective of flood risk in the Skagit River Basin: Both studies explored the impact of climate change on discharge. Saucier and Dionne (1998), in a modeling study of the HBC, analyzed sea ice and oceanographic sensitivity to atmospheric forcing and runoff, including strong negative surface air temperature anomalies in response to strong northerly winds associated with a westerly phase of the North Atlantic Oscillation, extreme runoff events, regulation, doubling in storm intensity in fall, and increased warming. Results showed an increase in ice formation in winter due to regulation, in agreement with a one-dimensional mixed-layer model assessment outlined in Prinsenberg (1983). Also demonstrated was a slight increase in simulated SST in spring due to lower salinity with excess runoff in winter, followed by negative anomalies in summer associated with reduced runoff in summer due to regulation; enhanced simulated SSTs were generated under the influence of increased temperatures in summer.

In this study, we explored the relative and combined impacts of climate change and regulation on sea ice state and dynamics in the HBC and examined questions including: How is the annual cycle in sea ice and ocean conditions influenced by the impacts of climate change and regulation? Does regulation enhance or decrease climate change impacts? How will persistence in sea ice conditions be influenced by climate change and regulation impacts combined? Will a more diffusive (homogeneous) sea ice cover be attained? To address these questions in the context of BaySys objectives, we analyze output from simulations implemented for the BaySys project. These simulations use atmospheric and discharge forcing with the Nucleus for European Modelling of the Ocean (NEMO)

model (as described in Stadnyk et al., 2021, and Braun et al., 2021), through a spatiotemporal evaluation of

1. Climate change (CC) impacts on marine (SST, sea ice) conditions based on comparison between historical (1981–2010) and future (2021–2050 and 2041–2070) ice and ocean model output on monthly timescales;
2. Regulation (R) impacts on marine conditions based on comparison between historical, naturalized (river discharge without anthropogenic intervention) and regulated (river discharge with anthropogenic intervention, including dams, diversions, reservoirs), simulations on monthly timescales;
3. Combined regulation and climate change impacts on marine conditions based on comparison between future (2021–2050 and 2041–2070) naturalized and regulated regimes;
4. Relative contributions ($CC/[CC + R]$; $R/[CC + R]$) from climate change and regulation.

Data and methods used to achieve the evaluation and objectives are described in Section 2, the results and discussion of temporal, spatial, and persistence analyses for climate change, regulation, and combined regulated and climate change impacts are presented in Section 3, and a synopsis of relative climate change and regulation contributions, and implications, is outlined in Section 4.

2. Data and methods

2.1. Model output

The impacts of relative climate change and regulation are assessed using output from the Arctic and Northern Hemisphere Atlantic (ANHA) configuration of the NEMO v3.6 ocean/sea-ice coupled model, with 1/4-degree grid spacing for a horizontal resolution of 10–15 km in the HBC. The ANHA configuration was developed and implemented at the University of Alberta. Additional information about the ANHA configuration of the NEMO model, experimental design, and sensitivity studies may be found in Ridenour et al. (2019), Castro de la Guardia et al. (2019), Jafarikhasragh et al. (2019), Stadnyk et al. (2020), and Braun et al. (2021). Climate change impacts are evaluated through comparison of historical and future experiments defined by atmospheric forcing scenarios. For the BaySys project, atmospheric forcing includes three historical scenarios (Geophysical Fluid Dynamics Laboratory [GFDL], Meteorological Research Institute [MRI], and the Model for Interdisciplinary Research on Climate version 5 [MIROC5]; 1981–2005) and five future scenarios (GFDLrcp4.5, MRI rcp4.5 and rcp8.5, MIROC5 rcp4.5 and rcp8.5; 2006–2070) from the World Climate Research Programme Coupled Model Intercomparison Project Phase 5 (CMIP5). GFDL, MRI, and MIROC5 have atmospheric grid resolutions of $2^\circ \times 2.5^\circ, 1.1^\circ \times 1.1^\circ$, $1.4^\circ \times 1.4^\circ$, respectively. Atmospheric variables provided to the NEMO model include specific humidity, longwave and shortwave downwelling radiation, surface pressure, bias-corrected zonal and meridional winds, temperature, and precipitation (including snow). Additional information on CMIP5 scenario selection for the NEMO model (relative to scenario selection for the HYPE discharge model), differences between CMIP5 scenarios selected, and bias-correction techniques can be found in Braun et al. (2021).

Regulation impacts on freshwater-marine coupling and ice/ocean variables are assessed through comparison of naturalized and regulated simulations defined by discharge forcing. Historic and future naturalized HYPE discharge data were provided for the HBC and Arctic, and regulated data were provided for the HBC by the BaySys freshwater team. For each model, the monthly fields provided over 1980–2070 for the HYPE naturalized and regulated runoff scenarios (10 total) were regridded from the river mouth positions onto the NEMO model grid using the approach discussed in Hu et al. (2018) and Hayashida et al. (2019). Enhanced vertical mixing of 2×10^{-3} m^2 s^{-1} was applied within the same river mouth polygons for depths to 30 m in order to prevent unrealistic salinity values. Additional information regarding the HYPE model and its development (Stadnyk et al., 2020), regulated scenarios (Tefs et al., 2021), combined climate change and regulation scenarios (Stadnyk et al., 2021), analysis of naturalized and regulated historical and future experiments (Stadynk et al., 2021), and discharge uncertainty analyses (Lilhare et al. 2020; Pokorny et al., 2021) has been contributed to this special feature or published in other journals. An analysis of the impact of historical regulation within HB Rivers was reported by Déry et al (2018), and an impact assessment of 1.5°C and 2.0°C global warming on HB hydrology can be found in MacDonald et al. (2018).

In this study, SIC, SIT, zonal (u_{ice}) and meridional (v_{ice}) sea ice drift and SST are evaluated on monthly timescales to provide a sense of changes in sea ice state (SIC and SIT) and dynamics (u_{ice} and v_{ice}) over an annual cycle in response to climate change and regulation. Sea ice drift speed, $|\vec{u}| = \sqrt{{u_{\text{ice}}}^2 + {v_{\text{ice}}}^2}$, and the meridional circulation index (MCI), $\text{MCI} = \frac{v_{\text{ice}} * |v_{\text{ice}}|}{{u_{\text{ice}}}^2 + {v_{\text{ice}}}^2}$, following Frances et al. (2015) are evaluated for the temporal analysis as metrics for ice drift magnitude and direction. Zonal flow is depicted by $\text{MCI} = 0$,and northward (southward) drift by $\text{MCI} = 1(-1)$.Sea surface salinity and mixed layer depth are analyzed and results presented in the supplemental section as an example of application to other (in this case oceanographic) variables of interest. Sea ice area (cumulative concentration multiplied by grid cell size) and sea ice volume (SIT multiplied by concentration and grid cell size) are also analyzed to examine monthly differences in the ice cover and volume in response to climate change and regulation. Because "historical" CMIP5 scenarios are provided to 2005, while "future" CMIP5 scenarios begin in 2006, variables for the historical time frame in this analysis include those from the historical time frame (1981–2005) concatenated with those from the future time frame to 2010 (2006–2010). Simulations/experiments are then labeled accordingly for ease of comparison with the five future model runs; that is, the MRI historical

simulation becomes MRI4.5 and MRI8.5 with the addition of the five years from future CMIP5-forced NEMO runs, and NEMO naturalized and regulated simulations were each run continuously from 1981 to 2070. As noted below, the "historical" time frame for the BaySys project is selected as the 1981–2010 time interval according to BaySys objectives, to the 1981–2010 climatology, and to ensure consistency in analysis among all BaySys teams.

2.2. Methods

In order to evaluate impacts of projected climate change and regulation in the HBC, analysis is completed for historical (*H*; 1981–2010) and future (*P*; 2021–2050, *f*1, and 2041–2070, *f*2) naturalized (*N*) and regulated (*R*) experiments for the five CMIP5-forced NEMO model runs. Specifically, climate change (CC), combined climate change and regulation (CCpR), historical regulated (Rh), and cumulative regulated (Rc) impacts are evaluated as follows:

$$\mathrm{CC} = PN - HN;$$

$$\mathrm{CCpR} = PR - HR;$$

$$\mathrm{Rh} = HR - HN;$$

$$\mathrm{Rc} = \mathrm{CCpR} - \mathrm{CC},$$

where differences indicate comparisons between relevant simulations in order to estimate relative impacts. Specifically, CC depicts climate change impacts alone based on comparison of future and historical naturalized regimes, CCpR depicts combined climate change and regulation impacts based on comparison of future and historical regulated regimes, Rh indicates regulation impacts based on comparison of historical regulated and naturalized regimes, and Rc depicts cumulative regulation impacts based on the residual in the combined climate change and regulation impacts and climate change impacts alone. Rh, which is intended to identify the impacts of regulation uninfluenced by climate change, will be affected by differences in internal climate variability associated with naturalized and regulated simulations run separately. However, the cumulative regulation impact Rc, intended to identify cumulative (historical and future) regulation impacts, is computed as the residual in the difference within (rather than between) each naturalized and regulated simulation and thus may be considered a more reliable estimate of regulation impacts. Percent relative climate change and regulation impacts are computed as $(\mathrm{CC}/(|\mathrm{CC}| + |\mathrm{Rc}|)) \cdot 100$and $(\mathrm{Rc}/(|\mathrm{CC}| + |\mathrm{Rc}|)) \cdot 100$, respectively. Each is also multiplied by the sign of the change in CCpR to indicate whether the relative contribution from each reinforces or counteracts the projected combined climate change and regulation impacts.

Traditional diagnostics including time series, box plots, and Hovmöller plots (contour plots as a function of latitude or longitude and time) are used to provide a spatio-temporal characterization of monthly changes in oceanographic and sea ice variables in response to climate change and regulation. Also examined is the change in persistence or "memory" of marine variables using a diagnostic known as the e-folding time spatial distribution (EFSD) used in past studies to evaluate changes in the Beaufort Sea marginal ice zone (Lukovich and Barber, 2005). This diagnostic is implemented by computing temporal autocorrelations of SIC, SIT, u_{ice}, and v_{ice} anomalies at each grid point and corresponding e-folding times of mean values for the 30-year (historical or future) interval considered. The e-folding times in "weeks" (5-day means based on NEMO output frequency) are then mapped at each grid point to identify spatial distributions in timescales, and (nearshore and offshore) changes in response to both regulation and climate, with implications for prediction and planning applications. Additional and more concise descriptions are provided below.

The following provides a summary of methodological analyses used to characterize climate change and regulation impacts on marine conditions in the HBC, as a template for similar investigations.

Temporal

1. Difference time series and boxplots for
   a) Historic and future naturalized (CC)
   b) Naturalized and regulated historic (R)
   c) Historic and future regulated (CCpR)

for all CMIP5-forced NEMO model runs with uncertainty, and for (two-model) mean emissions scenarios with uncertainty

2. Percent climate change and regulation impacts for sea ice variables

Spatial

3. Hovmöller plots and differences between historic and future naturalized and regulated CMIP5-forced NEMO model runs (with uncertainty based on standard deviation $\sigma_{HN,HR}$ and $\sigma_{PN,PR}$, respectively), with total uncertainty $\sigma_{\mathrm{tot}} = \sqrt{\sigma_{HN,HR}{}^2 + \sigma_{PN,PR}{}^2}$
4. Hovmöller plots and differences between individual historic and future members of CMIP5-forced NEMO model runs, with uncertainty based on spatial variability for each, and total uncertainty computed as in 3.

EFSD (to monitor persistence)

5. CMIP5 EFSD for December to April time frame and standard deviation
6. Difference EFSD maps for
   a) Historic and future naturalized (CC)
   b) Naturalized and regulated historic (*R*)
   c) Historic and future regulated (CCpR)

The time series analysis depicts climate change and regulation impacts evident in individual simulations, as well as the mean impacts and results associated with two

emissions scenarios and futures (RCP4.5 and RCP8.5). Because only the RCP4.5 scenario is available for GFDL, and to ensure consistency in RCP4.5 and RCP8.5 comparisons, the mean change in variables in the time series analysis for each emissions scenario is based on two model runs (MIROC5 and MRI).

Furthermore, because the purpose of this study is to analyze relative contributions from climate change and river discharge regulation to changes in SST and sea ice variables based on comparison of historical and future naturalized and regulated river discharge regimes, results from all five simulations combined are evaluated in the spatial (Hovmöller and EFSD) analysis. Results from further decomposition to evaluate RCP4.5 and RCP8.5 emissions scenarios based on two-model means yield comparable results that highlight intensification of impacts with increased emissions (not shown).

2.3. Uncertainty analysis

In the time series analysis for each model run i and marine variable x_i of those evaluated (SIC, SIT, $|u|$, MCI, SST, melt and freeze onset dates), the standard deviation $\sigma(x_i)$associated with the 30-year mean $\langle x_i \rangle$was computed on monthly timescales to account for model interannual variability over the 30-year historical (1981–2010) and future (2021–2050, *f*1, and 2041–2070, *f*2) time frames. Both 30-year future intervals were selected to allow for comparison with the historical 30-year interval. The total error associated with each (two-model) mean emissions scenario j is expressed as $\sigma_{\mathrm{tot},j} = \frac{\sum_{i=1}^{N_j} \sqrt{\sigma(x_i)^2}}{N_j} + \Delta_j$, where $N_j = 2$. The first term on the right hand side depicts the mean in the standard deviation (computed for the 30-year mean) for each model run associated with the given emissions scenario, as a measure of interannual variability. The second term on the right hand side depicts the standard deviation for each mean (two-model) emissions scenario, as a measure of inter-model variability.

Uncertainty in CC and CCpR was determined according to the relation:

$$\sigma_{\mathrm{CC}} = \sqrt{{\sigma_{PN}}^2 + {\sigma_{HN}}^2},$$

$$\sigma_{\mathrm{CCpR}} = \sqrt{{\sigma_{PR}}^2 + {\sigma_{HR}}^2}$$

where $\sigma_{PN,PR,HN,HR}$indicates the uncertainty or standard deviation for the model run, $\sigma(x_i)$, or (two-model) emissions mean, $\sigma_{\mathrm{tot},j}$,in the relevant variable. Similarly, uncertainty in the cumulative or residual regulation contribution, Rc, is expressed as

$$\sigma_{\mathrm{Rc}} = \sqrt{{\sigma_{\mathrm{CC}}}^2 + {\sigma_{\mathrm{CCpR}}}^2}.$$

In addition, uncertainty in percent relative and climate change impacts is depicted as

$$\delta = \frac{1}{(y+z)^2}\left(\sqrt{\delta x^2 \cdot (y+z)^2 + x^2 \cdot (\delta y^2 + \delta z^2)}\right)$$

for $x \equiv \mathrm{CCorRc}; \delta x = \sigma_{\mathrm{cc}} \mathrm{or} \sigma_{\mathrm{Rc}}$, $y \equiv |\mathrm{CC}|; \delta y = \sigma_{\mathrm{cc}}$, and $z \equiv |\mathrm{Rc}|; \delta z = \sigma_{\mathrm{Rc}}$. These uncertainties accompany the Hovmöller plots and EFSDs. Standard deviation in the EFSD also illustrates inter-model variability.

The mean is used to represent historical and future values for each scenario, and the standard deviation to measure uncertainty. Alternative uncertainty measures are considered (Supplemental section, Figures S1–S4) and standard deviation selected as a measure of the uncertainty and range in the CMIP5-forced NEMO-simulated marine variables. Because seasons are changing and definitions for season differ based on application, results are presented for monthly timescales.

3. Results and discussion

3.1. Climate change and regulation impacts: Temporal

Comparison of mean naturalized historical and future CMIP5-forced NEMO simulations illustrates future climate change (CC) impacts in the near term ($f1 = 2021$–2050) and long-term ($f2 = 2041$–2070), denoted in **Figures 1** and **2** as $\Delta_{\mathrm{CC}f1}$and$\Delta_{\mathrm{CC}f2}$. As expected, continued warming results in increased SSTs, with a maximum increase in July and sustained increase to December (Figure S5): differences are projected for *f*1 (*f*2) on the order of 1°C (2°C) in June, and 2°C (3°C) or less from August onward, with larger increases for the higher emissions (RCP8.5) scenario (**Figure 1**). An increase in the range of possible outcomes is also evident for the *f*2 time frame depending on which model forcing data are used as well as emission scenario (**Figure 1**). Temporal analysis of sea surface salinity and mixed layer depth is presented in the supplemental section (Figures S6–S9).

In consideration of SIC and SIT, a decrease in sea ice area and volume is similarly anticipated, with maximum decreases in sea ice area in December and January, and in sea ice volume in May (Figure S10). Because there is no sea ice in HB from August to October, major changes in sea ice occur in winter (rather than summer). For the *f*1 (*f*2) time frame, maximum decreases in sea ice area on the order of $2 - 4(4 - 6) \times 10^5 \mathrm{km}^2$ are evident in December/January, while simulations suggest a maximum decline in sea ice volume on the order of 1–2 (3–5) $\times$ 10^5 km^3, with a large spread among models and larger decreases for the high-emissions (RCP8.5) scenario (**Figure 2**). Simulations further suggest maximum decreases in sea ice drift speed for the *f*1 (*f*2) time frame on the order of 1 (4) cm/s and enhanced meridional drift evident in the MCI in December, with decreases on the order of 0.2 (0.1) from January to March. Also of interest is the large uncertainty in each sea ice variable due both to interannual variability associated with each CMIP5-forced NEMO model simulation and inter-model variability.

Comparison of historical regulated and naturalized experiments indicates regulation impacts in the absence of climate change (Rh). Changes in spatially averaged SST and sea ice variables suggest a weak response to regulation, with values of approximately 1% and 2% or less, respectively (not shown). Comparison of historical and future regulated experiments, indicating the combined impact of climate change and regulation (CCpR), shows

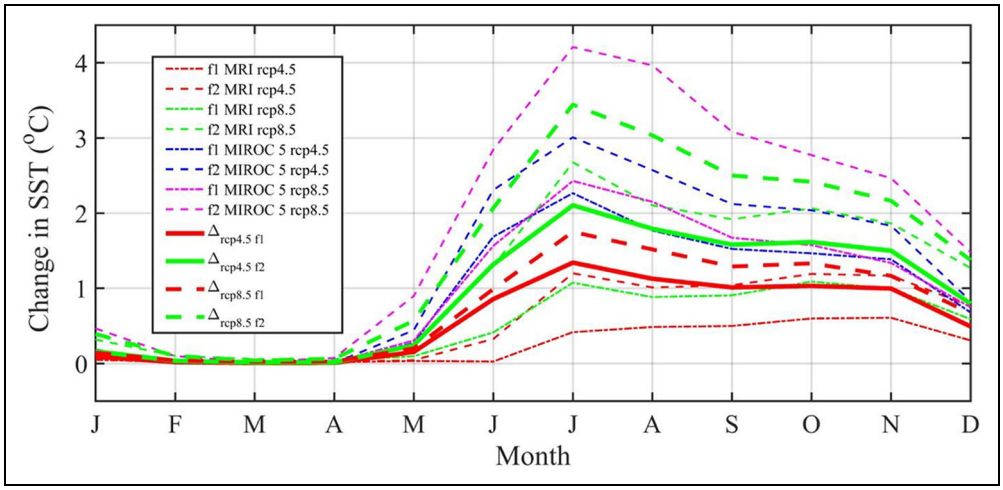

Figure 1. Difference in sea surface temperature from naturalized model simulations depicting climate change impacts. Sea surface temperature (SST) difference from naturalized CMIP5-forced NEMO simulations (MRI rcp4.5, MRI rcp8.5, MIROC5 rcp4.5, MIROC5 rcp8.5) for future time frames, denoted as *f*1 for 2021–2050 and *f*2 for 2041–2070, to characterize climate change impacts. Differences are based on the relation *PN* − *HN* (see Section 2.2). Differences associated with individual members are depicted by dash-dot lines as specified on the figure. CMIP5-forced two-model (MIROC5 and MRI) mean difference values for the RCP4.5 (RCP8.5) scenario are depicted by heavy solid (dashed) lines for the *f*1 (red) and *f*2 (green) time frames. NEMO = Nucleus for European Modelling of the Ocean; CMIP5 = Coupled Model Intercomparison Project Phase 5. DOI: https://doi.org/10.1525/elementa.2020.00127.f1

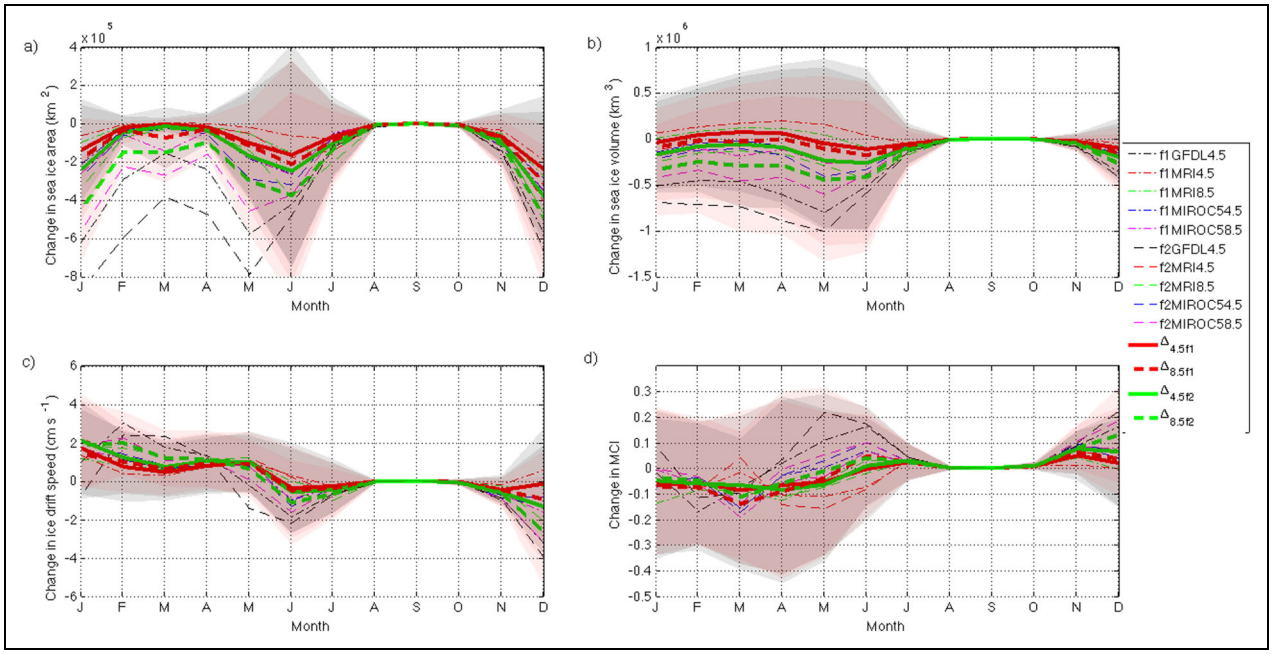

Figure 2. Differences in sea ice variables from naturalized model simulations depicting climate change impacts. Differences in (a) sea ice area (km^2), (b) sea ice volume (km^3), (c) sea ice drift speed (cm s^{-1}), and (d) meridional circulation index from naturalized CMIP5-forced NEMO simulations (GFDL rcp4.5, MRI rcp4.5, MRI rcp8.5, MIROC5 rcp4.5, MIROC5 rcp8.5) for future time frames, denoted as *f*1 for 2021–2050 and *f*2 for 2041–2070, to characterize climate change impacts. Differences are based on the relation *PN* − *HN* (see Section 2.2). Differences associated with individual members are depicted by dash-dot lines as specified on the figure. CMIP5-forced two-model mean RCP4.5 (RCP8.5) difference values are depicted by the heavy solid (dashed) lines for the *f*1 (red) and *f*2 (green) time frames. Shading depicts total uncertainty as measured by standard deviation for the individual simulations, depicting interannual variability (dark), and the standard deviation for the emission-scenario means, depicting inter-model variability (light). NEMO = Nucleus for European Modelling of the Ocean; CMIP5 = Coupled Model Intercomparison Project Phase 5; GFDL = Geophysical Fluid Dynamics Laboratory; MRI = Meteorological Research Institute; MIROC5 = Model for Interdisciplinary Research on Climate version 5. DOI: https://doi.org/10.1525/elementa.2020.00127.f2

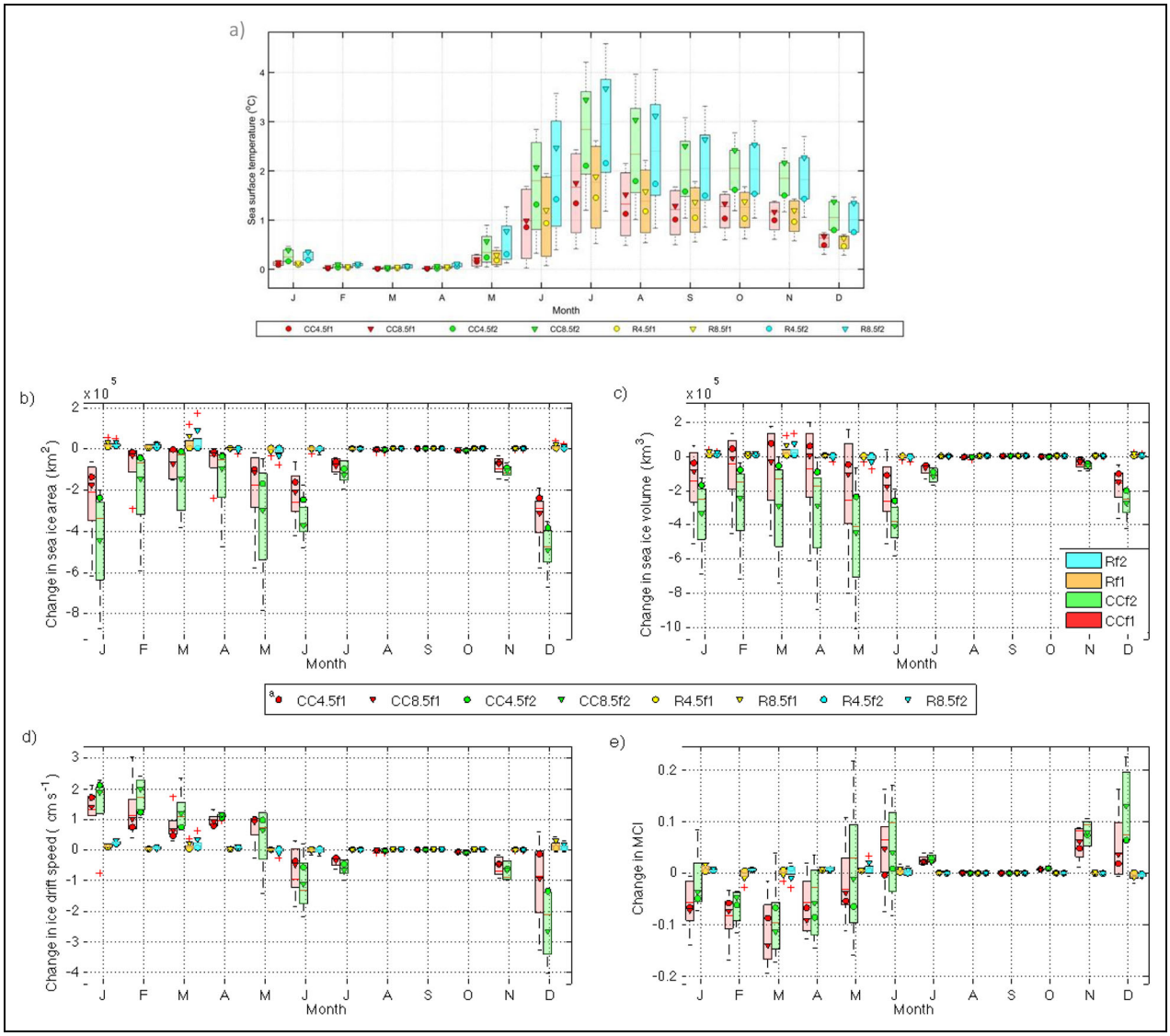

Figure 3. Differences in regime variables between historical and future naturalized and regulated model simulations. Climate change and regulation impacts based on differences between mean 30-year historical and future naturalized and regulated simulations for spatially averaged (a) sea surface temperature, (b) sea ice area, (c) sea ice volume, (d) sea ice drift speed, and (e) the meridional circulation index. Box plots depict differences between the historical and future naturalized and regulated regimes associated with all 5 model simulations, with red (orange) shading depicting climate change (regulation) impacts during the *f*1 time frame (2021–2050), and green (cyan) shading depicting climate change (regulation) impacts during the *f*2 time frame (2041–2070). Symbols depict climate change and regulation impacts associated with the two-member model mean for the RCP4.5 and RCP8.5 scenarios during the *f*1 and *f*2 time frames, as specified in the horizontal legend. Red crosses indicate outliers, while box edges depict upper and lower quartiles, and central lines the median; whiskers identify the range defined by values not considered to be outliers. DOI: https://doi.org/10.1525/elementa.2020.00127.f3

differences in SST and sea ice variables comparable to those for CC. The residual determined from comparison of CCpR and CC indicates regulation impacts in the presence of climate change (Rc) and captures current and future conditions in the HBC.

Despite similar behavior in SST and sea ice variables for CC and CCpR, slight differences due to regulation are highlighted in the comparison of CC and Rc (**Figure 3**). Specifically, slight increases in SSTs occur from April to August, with an increase in the SST maximum in June and July during the *f*2 time frame that is amplified for the mean RCP8.5 emissions scenario. In addition, simulations suggest that decreases in sea ice area and volume are weaker in response to climate change and regulation than in response to climate change alone in March, indicating that during this month regulation suppresses climate change impacts, particularly for the RCP8.5 emissions scenario (**Figure 3**). Regulation is also shown to oppose changes in ice drift speed due to CC in December and reinforce them in January and March. Regulation further opposes changes in meridional circulation due to CC in January, May, and to a lesser extent December. Overall, however, the spatially averaged CC effect dominates the R effect by approximately an order of magnitude for all variables.

These results agree in large part with previous studies that showed enhanced ice formation in winter due to regulation (Prinsenberg, 1983; LeBlond et al., 1996; Saucier and Dionne, 1998). In particular, LeBlond et al. (1996) found that hydroelectric regulation resulted in an increase in ice formation due to an extension in under-ice plumes associated with enhanced discharge in winter; such plumes may have a greater impact in a changing climate that increases both the magnitude and spatial extent of regulation impacts offshore. An increase in sea ice area of 20,000–30,000 km^2 found in the present study is consistent with the increase of $23,000$ km^2 documented in LeBlond et al. (1996) from regulation of all rivers in the HBC.

Previous studies have also highlighted the increasingly important role of freshwater discharge due to runoff in the Arctic in summer (Morison et al., 2012; Nghiem et al., 2014), describing the entrainment of warm plumes as pulses of freshwater are released from a sudden disintegration in ice barriers. Déry et al. (2016) further demonstrated enhanced discharge for the La Grande Rivière and Nelson River over the past several decades due to diversions that result in increased flow in all seasons. Increased SSTs from April to August due to regulation, contrary to past studies noting a decrease in surface temperatures due to a decrease in discharge in summer with regulation (Prinsenberg, 1983; Saucier and Dionne, 1998), suggest that diversions in the HBC contribute to increased flow in summer, possibly associated with increasing diverted flow volumes to compensate for decreasing summer flows projected under climate change (in the Nelson and other regulated rivers) in order to maintain optimal operating levels, as described in Stadnyk et al. (2021). Additional interpretations are that (i) regulation gives rise to increased SSTs due to increased stability and warming of the upper layer due to a stable thin mixed layer associated with extended under-ice plumes, or (ii) climate change impacts in the form of enhanced melt and increased freshwater release due to climate change in summer overwhelm negative SST anomalies associated with regulation and decreased discharge in summer documented in earlier studies.

Cumulative regulation (Rc) contributions are depicted in a summary of percent climate change and regulation impacts on sea ice variables in the HBC for the $f1$ and $f2$ time frames and mean RCP4.5 and RCP8.5 emissions scenarios (**Figure 4**). Percent changes are multiplied by the sign of the change in the combined climate change and regulation impacts to indicate whether the response reinforces or opposes the combined impact (i.e., negative Rc percent values indicate that regulation counteracts the change in sea ice variables). Transparency characterizes sea ice occupancy (the ratio of grid cell count with SICs exceeding 15% to total grid cell count for the HBC) for the combined climate change and regulation regime. Percent Rc impacts are less than 5% (dropping to −30% and below) in March in sea ice area and volume for the mean RCP4.5 (RCP8.5) emissions scenario. In consideration of sea ice drift speed, percent Rc impacts are on the order of 10% (30%) or less for the RCP4.5 (RCP8.5) emissions scenario; regulation suppresses climate change impacts in December, while reinforcing them in January and March. Percent Rc impacts counteract CC impacts for MCI in January and May, with values on the order of 5%–10% (10%–20%) and 5% (30%), respectively, for the mean RCP4.5 (RCP8.5) emissions scenario. Regulation reinforces climate change impacts on circulation in March for the RCP8.5 scenario, with values ranging from 5% to 10% during the $f1$ and $f2$ time frames. Spatial distributions and regional variability in relative CC and Rc impacts are explored in the following sections.

3.2. Spatial

Comparison of historical and future naturalized and regulated experiments from the perspective of longitudinal and latitudinal variations in sea ice variables using Hovmöller diagrams illustrates spatial and regional variability in sea ice response to climate change and regulation (**Figures 5**–**7**). Hovmöller diagrams of sea ice variables for historical and future naturalized and regulated regimes may be found in the supplemental section (Figures S11 and S12).

Evaluation of climate change impacts alone shows that SIC is projected to decrease by approximately 20% in central HB in December and January (**Figure 5e**) and in southwestern HB in May for the $f1$ time frame (**Figure 5a**). Maximum decreases in simulated SIT exceeding approximately 50 cm are evident in southern and central HB in May (**Figure 5b**), with larger decreases in eastern than western HB from May to June (**Figure 5f**). Reduced cyclonic circulation in December, evident in negative changes in zonal ice drift (**Figure 5c** and **g**) and positive changes in meridional ice drift (**Figures 5d** and **h**), is also observed. These results further suggest enhanced cyclonic circulation in January, evident in positive changes in zonal ice drift and negative changes in meridional ice drift, in southwestern HB in response to CC impacts alone. Specifically, reduced zonal drift is evident in December (–2 cm/s), and enhanced zonal drift in January, February, and April (2 cm/s); reduced meridional drift, characteristic of reversals, is evident in December (1–2 cm/s), and enhanced meridional drift in January and May (1–2 cm/s). Noteworthy is the east-west asymmetry in changes in sea ice drift, depicted by the reversal in sign in change in vice in May and June (**Figure 5h**). A similar result was documented in Hochheim and Barber (2010) and described in recent ice thickness and circulation studies (Landy et al., 2017; Kirillov et al., 2020). Furthermore, reduced southward (northward) drift is evident in western (eastern) HB, in a manner consistent with MCI results (**Figure 3**), in December, May, and to a lesser extent June.

Changes in sea ice conditions for Rh, Rc, and CCpR depict contributions from regulation that reinforce and counteract CC impacts (Figures S14–S16). Evaluation of river regulation alone and combined climate change and regulation impacts indicates that regulation weakly counteracts sea ice loss due to CC in January, February, and most notably March, as demonstrated by an increase in SIC of approximately 5% and SIT of approximately 5 cm throughout the HBC and especially in eastern HB (Figures S15 and S16). Regulation counteracts CC effects on sea ice

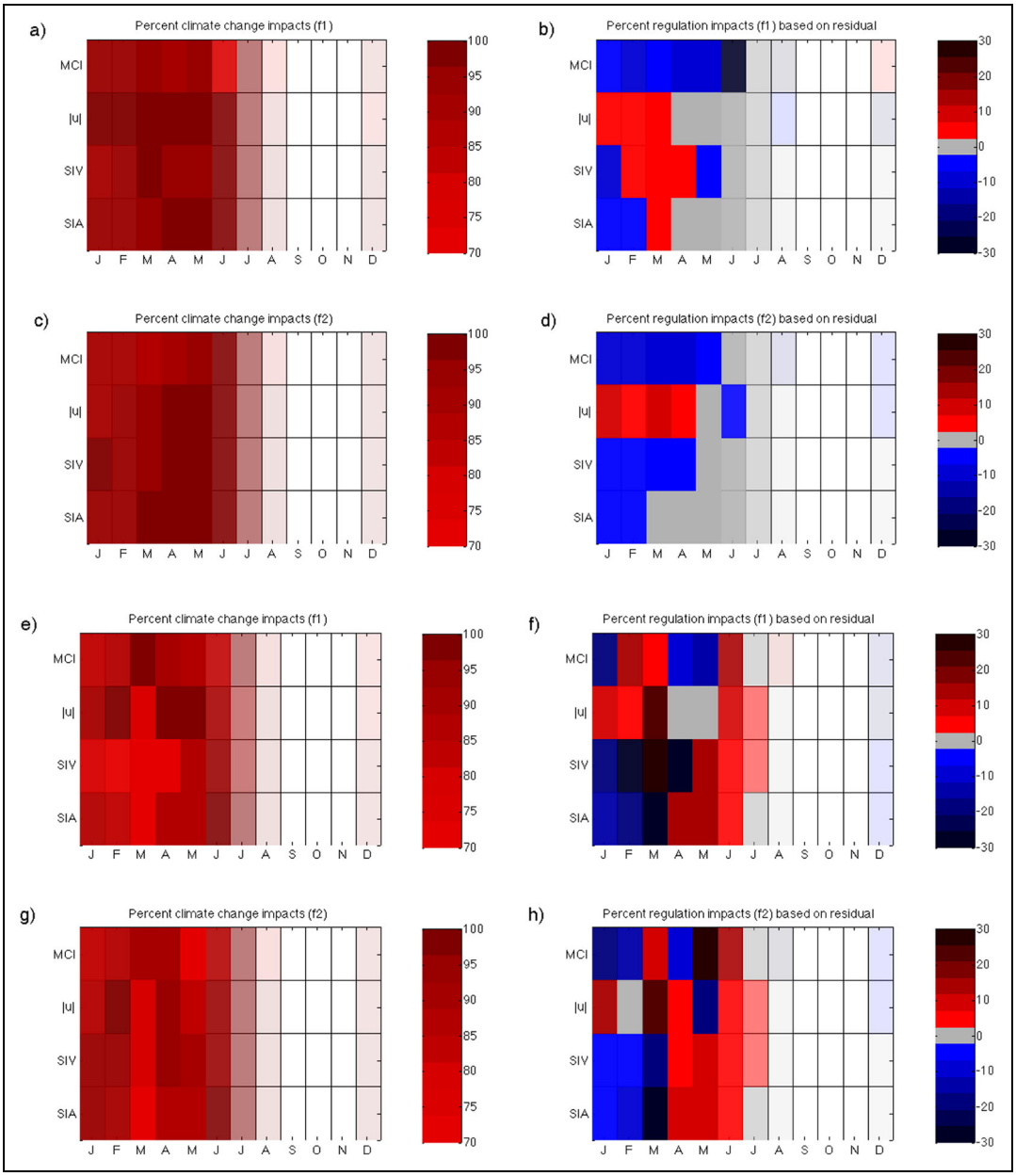

Figure 4. Percent climate change and regulation impacts for regime variables by month. Each panel depicts impacts for sea ice area (SIA), volume (SIV), mean sea ice drift speed ($|\vec{u}|$), and the meridional circulation index (MCI) on a monthly timescale. Left panels depict percent climate change impacts for the two-member RCP4.5 scenario mean for (a) *f*1 (2021–2050) and (c) *f*2 (2041–2070) and RCP8.5 scenario mean for (e) *f*1 and (g) *f*2. Right panels similarly depict percent regulation impacts for the two-member RCP4.5 for (b) *f*1 and (d) *f*2 and RCP8.5 for (f) *f*1 and (h) *f*2 determined from the residual in the climate change (CC) and combined climate change and regulation (CCpR) impacts (see Section 2.2). Negative values in the right panels indicate impacts that counteract combined climate change and regulation impacts. Color transparency (between July and December) depicts the ratio of grid cell count with SICs exceeding 15% to total grid cell count comprising the HBC region of interest over which variables are averaged, for the combined climate change and regulation regime. Grey shading depicts zero change in the presence of sea ice, while white areas depict an absence of sea ice (SIC less than or equal to 15%). SIC = sea ice concentration; HBC = Hudson Bay Complex. DOI: https://doi.org/10.1525/elementa.2020.00127.f4

dynamics in December (with $\Delta u_{ice} > 0$ and $\Delta v_{ice} < 0$), and in January (with $\Delta u_{ice} > 0$ and $\Delta v_{ice} > 0$) associated with increased zonal flow that disrupts meridional circulation. Similar yet amplified behavior in sea ice variables is projected for the *f*2 time frame (Figures S17 and S18).

Percent climate change (CC) and regulation (Rc) impacts during the *f*1 time frame highlight contributions from regulation to increases in SIC and SIT in January, February, and March, with maximum contributions in March that extend offshore, as demonstrated in the yellow band of approximately 30% Rc contributions extending westward from 74°W from January to March (**Figure 6p**, upper array (I)). Weaker contributions (approximately 20%) to increases in SIC and SIT are also observed in

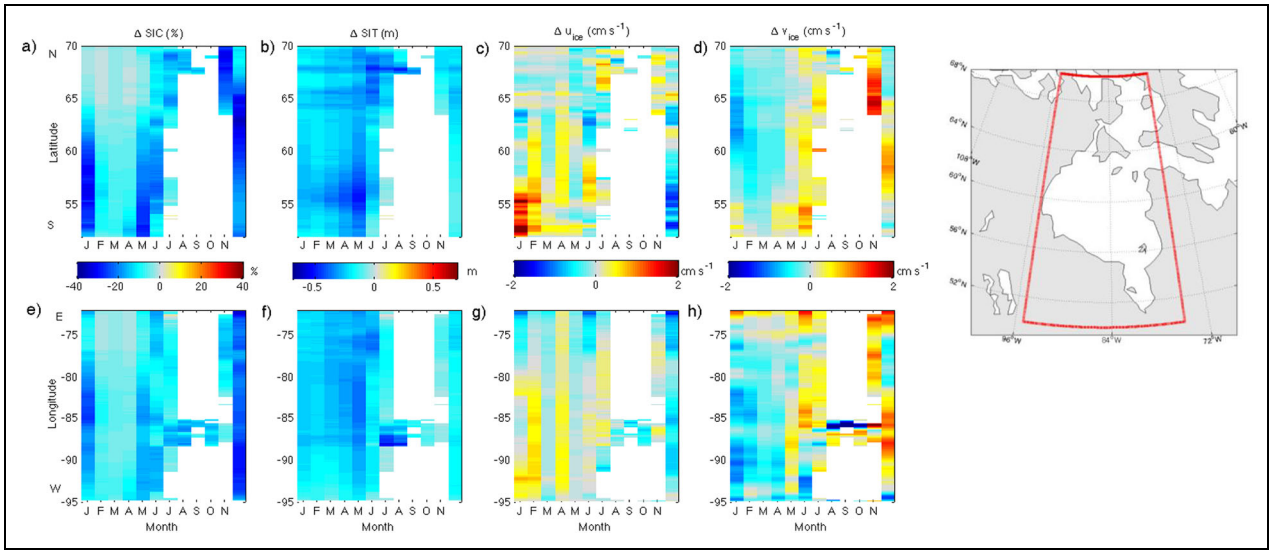

Figure 5. Hovmöller plots of changes in regime variables by month in response to climate change impacts. Depicted are changes in (a, e) sea ice concentration (SIC; in %), (b, f) sea thickness (SIT; in m), (c, g) zonal sea ice drift (u_{ice}; in cm s^{-1}), and (d, h) meridional sea ice drift (v_{ice}; in cm s^{-1}) on a monthly timescale in response to climate change impacts based on comparison of the future (*f*1; 2021–2050) to the historical (1981–2010) time frame for naturalized regimes. Upper panels depict zonally averaged values; lower panels indicate values averaged over all latitudes from 52°N to 70°N, as shown in the inset map. Only those regions where SIC exceeds 15% are shown in the Hovmöller plots. DOI: https://doi.org/10.1525/elementa.2020.00127.f5

southwest HB in June. As previously noted, regulation is shown to counteract CC effects and enhance cyclonic circulation in December. This counteraction is evident in negative changes in v_{ice} (approximately 30%; **Figure 6c** and **d**), and positive changes in u_{ice} (**Figure 6g** and **h**), throughout most of the HBC. Furthermore, regulation is shown to suppress enhanced cyclonic circulation attributed to CC in HB in January due to enhanced zonal drift (**Figure 6g** and **h**). This suppression is evident in contributions on the order of and/or exceeding 50%. Similar yet amplified results are observed for percent contributions during the *f*2 time frame (Figure S19). Maximum uncertainty is found for zonal and meridional sea ice drift, as expected due to variability on monthly timescales (**Figures 7** and S20).

In summary, spatial analysis of the relative contributions of climate change and river regulation to changes in SIC, SIT, zonal, and meridional sea ice drift demonstrates that cumulative regulation suppresses sea ice loss (in concentration and thickness) by approximately 30% relative to total climate change and regulation contributions throughout HB in January, February, and March. It weakens cyclonic circulation by approximately 50% in January due to enhanced zonal drift, particularly in southwestern HB.

3.3. EFSD

How is persistence in sea ice conditions influenced by climate change and regulation? EFSDs in winter (December to April) for each variable anomaly during the mean historical (*f*1) and future (*f*2) time frames in the naturalized flow regime illustrate a degradation in persistence due to the influence of climate change (**Figure 8**). Specifically, simulations suggest that patterns indicating a 4-week persistence in SIC in central and northwestern HB during the historical time frame are eroded in the *f*1 time interval and partially recovered in western HB in the *f*2 time interval as the marine system adapts to a new ice regime. Similarly, persistent (approximately 10 weeks) SIT in central and southeastern HB during the historical time frame is replaced with a heterogenous pattern of shorter memory coherent features distributed throughout southeastern HB in *f*1, and EFSD values less than 5 weeks in the same region in *f*2, with an approximate 7-week remnant located in north-central and western HB. During the historical time frame, HB is characterized by a zonal ice drift 2-week (1-week) EFSD pattern in northwestern (southeastern) HB that is replaced by a comparatively homogeneous distribution of low EFSD values in the *f*1 and *f*2 time frames, indicative of a transition to shorter temporal and spatial correlations. Finally, lower persistence values in meridional ice drift in northwestern HB in the historical era characteristic of polynya openings/closings and northwesterly winds that would interrupt southward drift in this region are replaced by 2-week persistence in western and southwestern HB in *f*1, in keeping with enhanced cyclonic circulation observed for CC impacts, and shorter timescales in central HB in *f*2; the latter may be attributed to enhanced response of a thinner sea ice cover to atmospheric forcing and local-scale processes within a new sea ice regime. Differences between simulations are depicted in the standard deviation in EFSDs for the historical and future naturalized regimes, capturing inter-model variability (Figure S21).

Changes in EFSDs based on comparison of historical and future naturalized regimes highlight the impact of

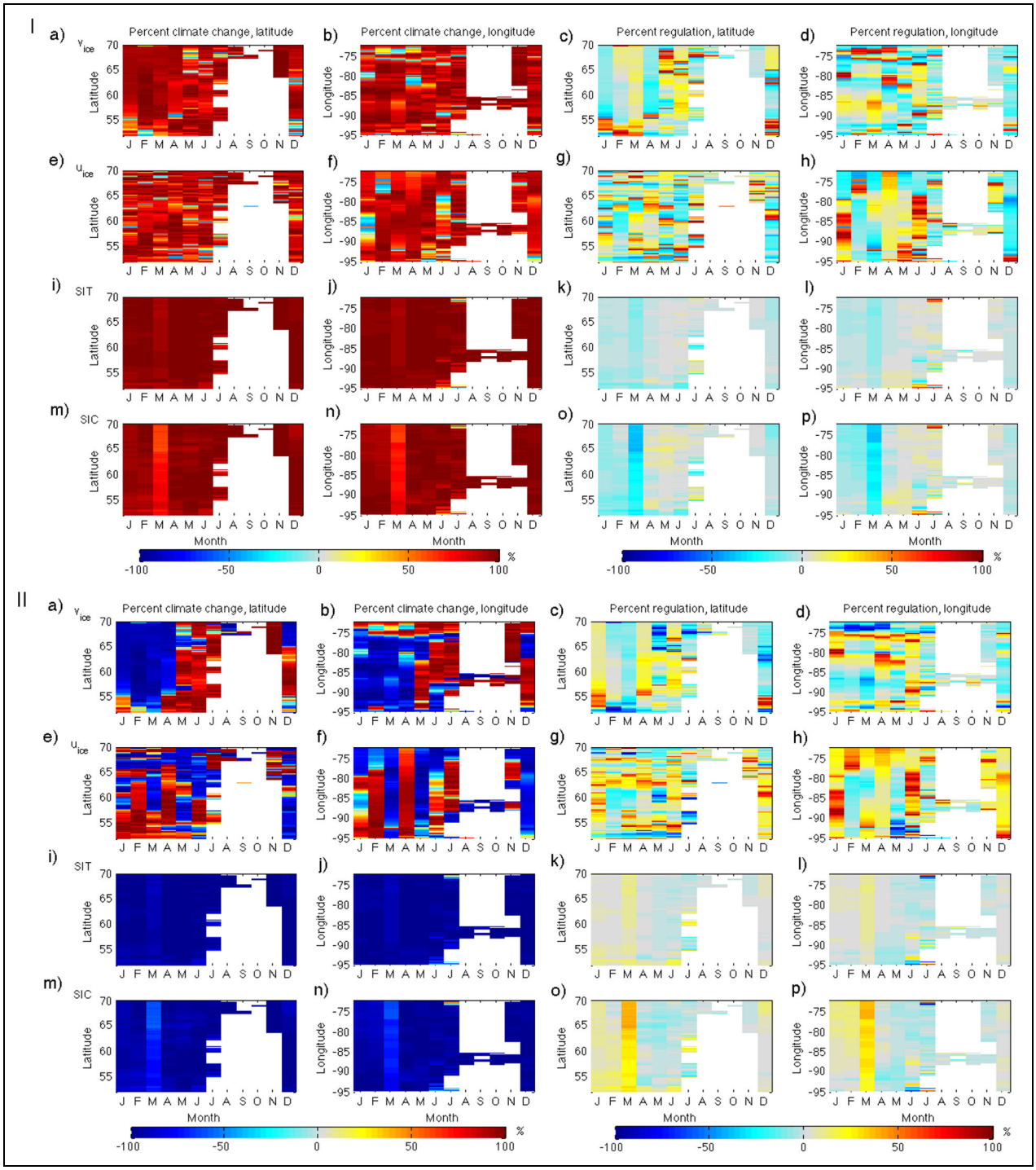

Figure 6. Hovmöller plots of percent climate change and regulation impacts on variables by latitude/longitude and month. Depicted are percent climate change (CC) and regulation (Rc) impacts as a function of latitude and longitude on regime variables, from lowest to uppermost row, sea ice concentration (SIC), thickness (SIT), zonal sea ice drift (u_{ice}), and meridional sea ice drift (v_{ice}) on a monthly timescale for the *f*1 time frame (2021–2050). The left two columns depict percent climate change impacts; the right two columns, percent regulation impacts. Negative values indicate change opposite to the combined climate change and regulation impacts; that is, negative values in climate change or regulation impacts indicate negative (positive) contributions to positive/increasing (negative/decreasing) change in response to climate change and regulation combined. The residual in this figure is computed as the difference in change due to CC and combined climate change and regulation (CCpR) impacts, indicated in the upper array (I); the lower array (II) indicates the actual difference. DOI: https://doi.org/10.1525/elementa.2020.00127.f6

climate change on persistence of sea ice conditions (**Figure 9**). Demonstrated in particular is a 2-week reduction in SIC persistence in northern HB, and in SIT in northwestern and southeastern HB. A slight increase in persistence is observed offshore in northwestern HB near 60°N, 90°W, which may be indicative of repeated polynya

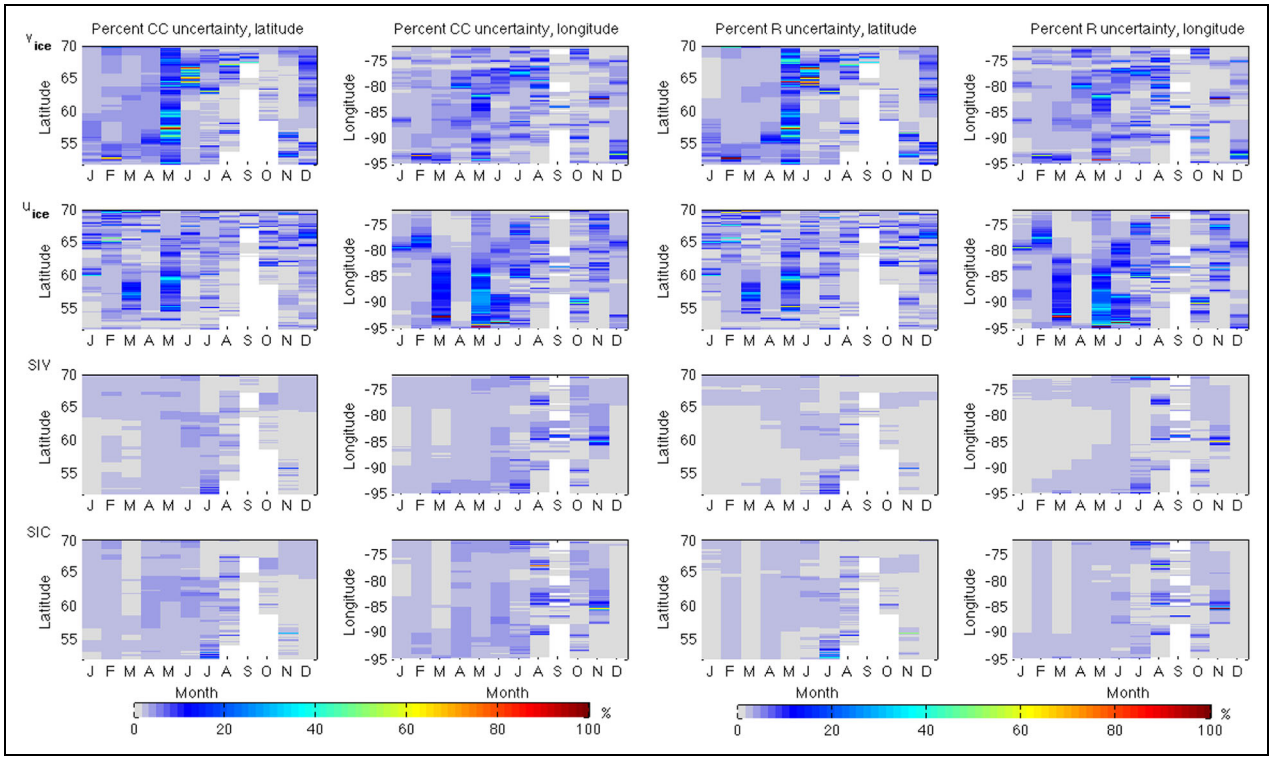

Figure 7. Hovmöller plots of percent uncertainty in climate change and regulation impacts on regime variables. Depicted are percent uncertainty in climate change (CC) and regulation (Rc) impacts as a function of latitude and longitude on regime variables, from lowest to uppermost row, sea ice concentration (SIC), thickness (SIT), zonal sea ice drift (u_{ice}), and meridional sea ice drift (v_{ice}) on a monthly timescale for the $f1$ time frame (2021–2050). Uncertainty in climate change impacts is determined from the standard deviation in the 5 CMIP5-forced NEMO simulations. Uncertainty in regulation impacts, defined as the residual in the climate change and combined climate change and regulation impacts, is determined as the square root in the sum of the squares in the latter. Total uncertainty is determined from error propagation. CMIP5 = Coupled Model Intercomparison Project Phase 5; NEMO = Nucleus for European Modelling of the Ocean. DOI: https://doi.org/10.1525/elementa.2020.00127.f7

opening and closing and refreezing of flaw leads that would increase persistence of ice behavior in this region. A decrease (increase) in persistence in zonal ice drift is projected for western (eastern) HB as a thinner and weaker ice cover becomes more susceptible to atmospheric forcing, while enhanced (reduced) persistence in meridional circulation is detected in western (eastern) HB as thinner ice is advected more freely in response to a changing climate. Behavior for $f2$ reflects an increase in SIC, intensified increase and decrease in SIT and zonal drift, and degradation in meridional drift persistence and EFSD patterns.

Changes in EFSDs based on comparison of historical regulated and naturalized regimes show a weak increase in persistence in SIC and SIT in nearshore northwestern HB in response to historical regulation (Rh), as would be expected with modulated river discharge, and declines in persistence in central HB (Figure S22). Enhanced persistence in zonal sea ice drift is evident nearshore in western HB due to changes in river discharge, with a low (high) persistence regime in central (eastern) HB in response to regulation; apart from reduced persistence in meridional ice drift in northwestern HB that may be indicative of interrupted inflow/outflow processes in this region in response to regulation, as well as remnants of reduced (enhanced) persistence in nearshore western and eastern (nearshore northern and offshore western) HB that may also be attributed to differences in discharge associated with regulation, no distinctive coherent regional-scale patterns in EFSD in meridional drift for the historical regulation regime are evident. By contrast, enhanced persistence in SIC and SIT is observed throughout HB under the influence of cumulative regulation (Rc) impacts as determined from the difference between CC and CCpR EFSDs in the $f1$ time frame (Figure S23). Enhanced persistence in zonal ice drift exists in northwestern HB, which may be attributed to enhanced zonal flow and influence associated with regulated discharge in winter (April to May), while reduced persistence in meridional ice drift suggests interruptions to southward advection due to cross-shear flow associated with discharge. Of interest is the EFSD pattern of enhanced/reduced persistence in zonal ice drift in central HB. Although zonal ice drift memory does not appear to change significantly during the $f2$ time frame, persistence in SIC and SIT deteriorates throughout the HBC and in northwestern HB, respectively, within this time frame, while persistence in meridional drift in northwestern HB increases, perhaps indicating enhanced response to northwesterly winds within a new ice regime.

EFSDs for sea ice variables for the historical and future time frames in the regulated regime show weaker

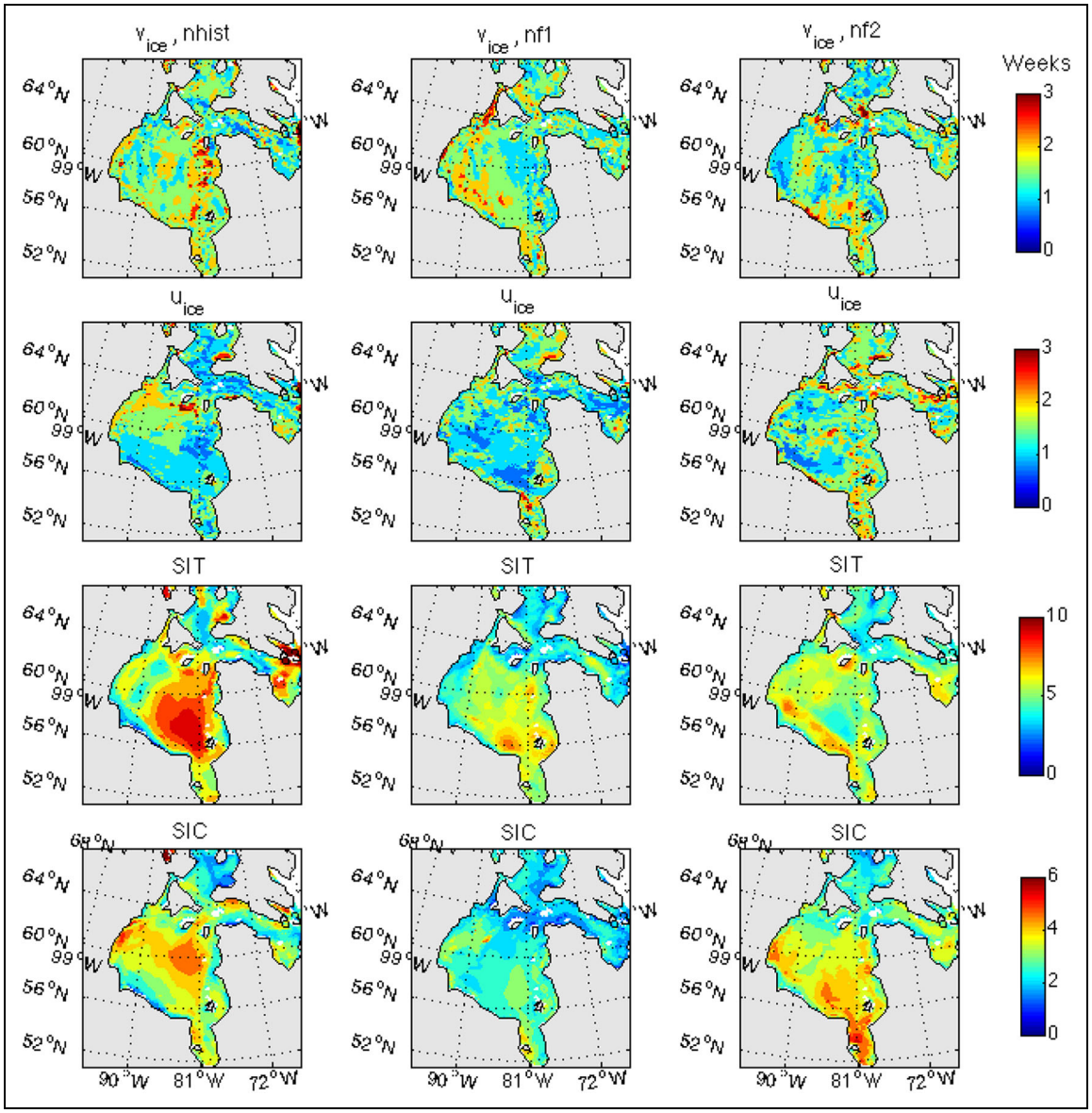

Figure 8. Persistence for regime variables during winter for historical and future naturalized model simulations. E-folding time spatial distribution (diagnostic for persistence) for regime variables, from lowest to uppermost row, sea ice concentration (SIC), thickness (SIT), zonal sea ice drift (u_{ice}) and meridional sea ice drift (v_{ice}), showing persistence or memory in each variable during winter (December to April) for, from left to right column, the historical (1981–2010) and future ($f1$, 2021–2050, and $f2$, 2041–2070) naturalized (n) regimes. Units are in weeks, where "week" refers to 5 rather than 7-day intervals based on model output frequency. DOI: https://doi.org/10.1525/elementa.2020.00127.f8

gradients between persistence patterns relative to the naturalized regime due to a changing climate (Figure S24) and uncertainty (Figure S25). This effect is further reflected in difference maps highlighting the combined impacts of climate change and regulation (Figure S26), with differences in the CC and CCpR scenarios captured in the residual (Rc) characteristic of cumulative regulation, particularly in northwestern and central HB (Figure S23). Percent regulation impacts show approximately 30% contribution to increased persistence in SIC and SIT throughout HB, and contributions of approximately 50% to increased persistence in SIT in northwestern HB (perhaps due to enhanced ridging with changes in river discharge combined with the effects of polynya formation), with 50% increase in persistence in zonal ice drift in central and northwestern HB and approximately 30% suppression in meridional drift for the $f1$ interval (**Figure 10**). These results are in contrast to the $f2$ time frame where regulation contributes to suppression in SIC and SIT persistence in northwestern HB and enhanced SIT in eastern HB. Uncertainty estimates demonstrate values on the order of 10% for appreciable climate and regulation contributions (**Figure 11**), with enhanced uncertainty for the $f2$ time frame, as anticipated.

In summary, evaluation of EFSD to understand how persistence in simulated sea ice variables is influenced by climate change and regulation shows that regulation alone acts to prolong persistence in SIC and SIT

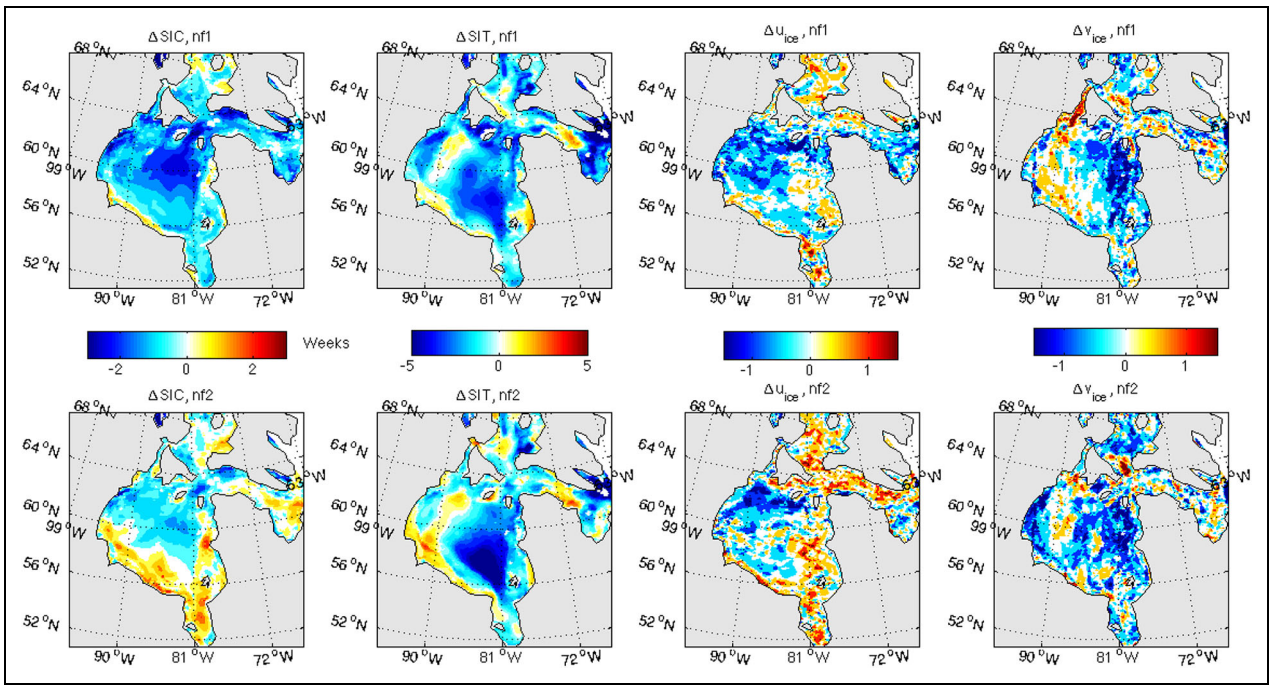

Figure 9. Change in persistence for regime variables between historical and future naturalized model simulations. Change in e-folding time spatial distribution (diagnostic for persistence) for regime variables, left to right, sea ice concentration (SIC), thickness (SIT), zonal sea ice drift (u_{ice}), and meridional sea ice drift (v_{ice}), based on comparison between the *f*1 timescale (2021–2050, upper panels) or *f*2 timescale (2041–2070, lower panels) and historical naturalized (*n*) simulations, showing climate change impacts on persistence or memory in each variable in the HBC. Units are in weeks, where "week" refers to 5 rather than 7-day intervals based on model output frequency. HBC = Hudson Bay Complex. DOI: https://doi.org/10.1525/elementa.2020.00127.f9

throughout HB in the *f*1 time frame and to reduce persistence in both SIC and SIT in northwestern HB within a new, thinner ice regime. Climate change and regulation combined further act to erode the spatiotemporal gradients in nearshore and offshore characteristics, with implications for biogeochemical processes on local and regional scales, ocean–sea ice–atmosphere interactions on local scales, and understanding of spatiotemporal distribution of relevant timescales in the HBC associated with sea ice state and dynamics relevant for forecasting and prediction, including planning from the perspective of emergency preparedness, infrastructure development, and resilience building, design, and implementation.

4. Summary

In this study, we investigated the relative impacts of climate change and regulation on ocean and sea ice conditions in the HBC. A template for analysis was presented to characterize and standardize methods in identifying projected spatiotemporal changes in marine variables on monthly timescales.

Temporal analysis showed that climate change impacts ascertained through comparison of historical (1981–2010) and future (2021–2050 and 2041–2070) naturalized simulations are evident in SST increases of approximately 2°C–3°C in summer, with values ranging from 1°C to 3°C among the five CMIP5-forced NEMO simulations. Results from temporal analysis of sea ice conditions also demonstrated decreases in sea ice area of approximately 4×10^5 km^2 and in sea ice volume of approximately 1×10^5 km^3. For the *f*1 (*f*2) time frame decreases in sea ice drift speed of approximately 1 (4) cm/s and enhanced meridional drift from January to March evident in MCI decreases of 0.2 (0.1) were also observed. Large uncertainty suggests a wide range of possible outcomes on monthly timescales. For the regional average climate change dominates the signal with regulation having a minor effect. Exceptions are in sea ice area and sea ice volume in March, and in sea ice drift speed and the MCI in January. In particular, percent climate change and regulation contributions suggest Rc impacts of approximately –30% in March in sea ice area and volume, 10% (30%) in ice drift speed in January, and –5% to –10% (–10% to –20%) in MCI in January for mean RCP4.5 (RCP8.5) emissions scenario during the *f*1 time frame.

Spatial analysis provides an indication of where relative climate change and regulation impacts occur in the HBC and percent contributions of each. Investigation of climate change impacts alone shows that SIC is projected to decrease by approximately 20% in December and January, SIT by approximately 50 cm in southern and central HB, with larger decreases in eastern than western HB in summer, while cyclonic circulation, particularly in southwestern HB, is expected to increase in January. A spatial analysis of relative climate change and regulation contributions to changes in ice concentration and thickness and in zonal and meridional sea ice drift demonstrates that cumulative regulation suppresses sea ice loss by

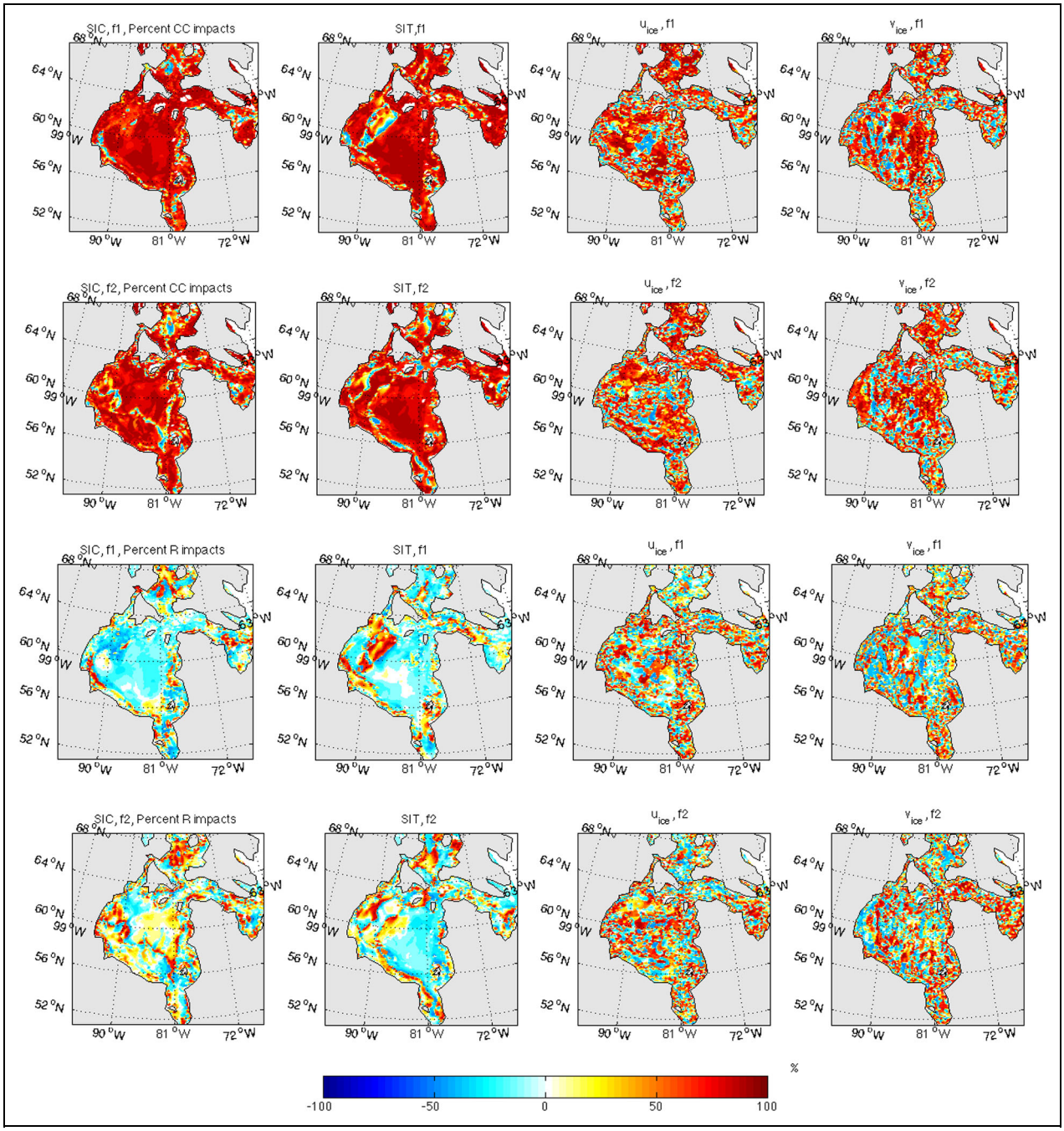

Figure 10. Percent relative climate change and regulation contributions to changes in persistence of regime variables. Contributions of percent relative climate change (CC, upper panels) for timescales *f*1 (2021–2050, top row) and *f*2 (2041–2070, second row) and regulation (*R*, lower panels) for *f*1 (third row) and *f*2 (bottom row) to changes in e-folding time spatial distribution (diagnostic for persistence) for regime variables, left to right, sea ice concentration (SIC), thickness (SIT), zonal sea ice drift (u_{ice}), and meridional sea ice drift (v_{ice}). Negative values indicate that the contribution counteracts the combined climate change and regulation impact (i.e., negative percent indicates a suppression of the variable persistence decrease). DOI: https://doi.org/10.1525/elementa.2020.00127.f10

approximately 30%, throughout HB in January, February and March, and weakens increases in cyclonic circulation by approximately 50% in January due to enhanced zonal drift, particularly in southwestern HB. In addition to demonstrating that regulation suppresses sea ice loss throughout the HBC in March, climate change acts to create spatial uniformity in regulation impacts and erode the distinction between nearshore and offshore processes, resulting in increased homogeneity in sea ice conditions, and amplification of regulation impacts offshore.

EFSDs provide a spatiotemporal estimate of changes in persistence in sea ice variables in response to a changing climate and regulation. Climate change is shown to erode persistence and EFSD patterns by up to 2 weeks in SICs in northern HB and in SIT in northwestern and southeastern HB and to induce an east-west asymmetry in zonal and

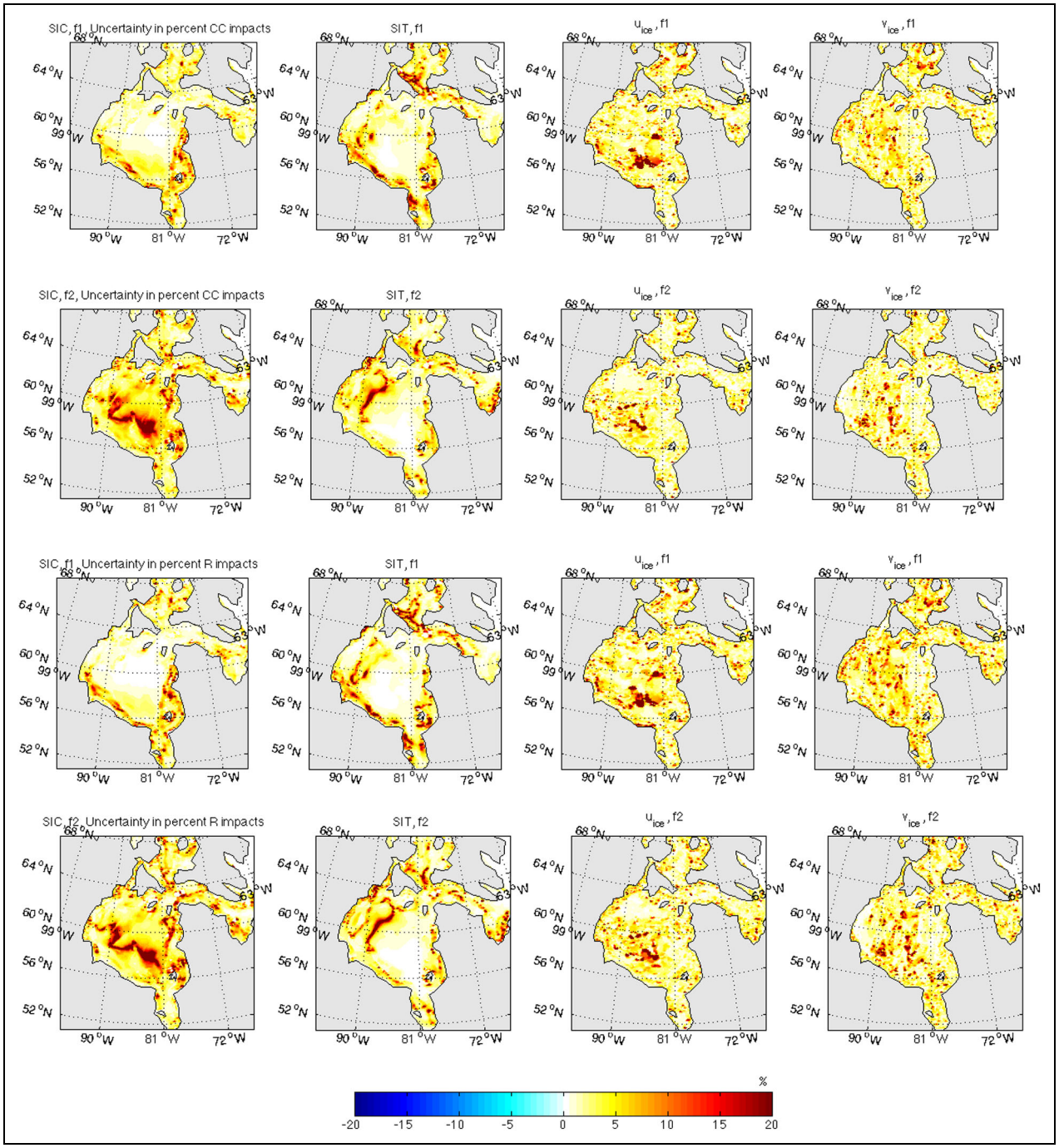

Figure 11. Uncertainty associated with percent relative climate change and regulation contributions to changes in persistence. Uncertainty associated with contributions of percent relative climate change (CC, upper panels) for timescales $f1$ (2021–2050, top row) and $f2$ (2041–2070, second row) and regulation (R, lower panels) for timescales $f1$ (third row) and $f2$ (bottom row) to changes in e-folding time spatial distribution (diagnostic for persistence) for regime variables, left to right, sea ice concentration (SIC), thickness (SIT), zonal sea ice drift (u_{ice}), and meridional sea ice drift (v_{ice}). DOI: https://doi.org/10.1525/elementa.2020.00127.f11

meridional sea ice drift response. Changes in EFSDs in response to regulation also indicate an increase in persistence in thickness offshore due to regulation, particularly in northwestern HB. Investigation of cumulative regulation (Rc) impacts determined from the residual in CC and CCpR shows reduced (weakly enhanced) persistence in SIC nearshore (offshore), similarly for SIT yet with enhanced reduction in SIT in central HB, enhanced zonal drift in northwestern and central HB and reduced meridional drift associated with cross-shear flow (from runoff) due to regulation. EFSDs as a map of timescales provide further evidence for erosion of a distinction between nearshore or offshore processes and extension of regulation impacts offshore. This erosion has implications for residence times associated with biogeochemical processes, sea ice formation and decay, and forecasting and prediction, while also

providing information on the timescales required for planning purposes.

Results from this analysis highlight that although climate change dominates SST and sea ice conditions, regulation can be important for regional changes in SICs and thickness in March and circulation changes in January and December due to enhanced zonal flow in southwestern HB. The EFSD analysis further illustrates that regulation can enhance persistence in SIC and thickness throughout HB, reduce this persistence in northwestern HB within a new, thinner ice regime, enhance zonal drift in northwestern and central HB, and disrupt meridional circulation. Furthermore, the template for analysis presented in this investigation can be used to analyze changes in other physical or biogeochemical variables and to characterize processes, including developing budgets, in response to the relative impacts of climate change and river regulation in the HBC, and thus help to inform planning, operations, preparedness, and responses to anticipated outcomes.

Data accessibility statement

All simulation output used in this research is available on Compute Canada (www.computecanada.ca) and made available through the BaySys data repository (http://lwbin-datahub.ad.umanitoba.ca/dataset/baysys-reports).

Supplemental files

The supplemental files for this article can be found as follows:

Figures S1–S26. Pdf

Acknowledgments

This work is a contribution to the Natural Sciences and Engineering Council of Canada (NSERC) Collaborative Research and Development project titled BaySys. In addition, this research contributes to the ArcticNet Networks of Centers of Excellence and the Arctic Science Partnership. The authors are grateful to editors Jody Deming and Stephen Ackley, and two anonymous reviewers, for constructive edits and suggestions that contributed to significant improvement of the manuscript.

Funding

Funding for this research was graciously provided by Manitoba Hydro, NSERC, Amundsen Science, and the Canada Research Chairs program.

Competing interests

The authors declare no competing interests.

Author contributions

Contributed to conception and design: JVL, SJ, KS, PGM, TAS.

Contributed to acquisition of data: PGM, TAS, NAR, LCG, XH, NG, JM, CP.

Contributed to analysis and interpretation of data: JVL, SJ.

Drafted and/or revised the article: JVL, SJ, JCS, PGM, KS, KW, TAS, LCG, XH, NG, NAR, JM, CP, DGB.

Approved the submitted version for publication: All authors.

References

Anctil, F, Couture, R. 1994. Cumulative impacts of hydroelectric development on the freshwater balance of Hudson Bay. *Canadian Journal of Civil Engineering* **21**: 297–306.

Arheimer, B, Donnelly, C, Lindström, G. 2017. Regulation of snow-fed rivers affects flow regimes more than climate change. *Nature Communications* **8**: 1–9.

Braun, M, Thiombiano, AN, Vieira, MJF, Stadnyk, TA. 2021. Representing climate evolution in ensembles of GCM simulations for the Hudson Bay System. *Elementa: Science of the Anthropocene* **9**(1). DOI: https://doi.org/10.1525/elementa.2021.00011.

Castro de la Guardia, L, Garcia-Quintana, Y, Claret, M, Hu, X, Galbraith, ED, Myers, PG. 2019. Assessing the role of high-frequency winds and sea ice loss on Arctic phytoplankton blooms in an ice-ocean biogeochemical model. *Journal of Geophysical Research: Biogeosciences* **124**: 2728–2750. DOI: http://dx.doi.org/10.1029/2018JG004869.

Déry, SJ, Mlynowski, TJ, Hernández-Henríquez, MA, Straneo, F. 2011. Interannual variability and interdecadal trends in Hudson Bay streamflow. *Journal of Marine Systems* **88**: 341–351.

Déry, SJ, Stadnyk, TA, MacDonald, MK, Gauli-Sharma, B. 2016. Recent trends and variability in river discharge across northern Canada. *Hydrology and Earth System Sciences* **20**: 4801–4818.

Déry, SJ, Stadnyk, TA, MacDonald, MK, Koenig, KA, Guay, C. 2018. Flow alteration impacts on Hudson Bay river discharge. *Hydrological Processes* **32**: 3576–3587. DOI: http://dx.doi.org/10.1002/hyp.13285.

Francis, JA, Vavrus, SJ. 2015. Evidence for a wavier jet stream in response to rapid Arctic warming. *Environmental Research Letters* **10**: 014005.

Gagnon, AS, Gough, WA. 2006. East-west asymmetry in long-term trends of landfast ice thickness in the Hudson Bay region, Canada. *Climate Research* **22**: 177–186.

Hayashida, H, Christian, JR, Holdsworth, AM, Hu, X, Monahan, AH, Mortenson, E, Myers, PG, Riche, OGJ, Sou, T, Steiner, NS. 2019. CSIB v1 (Canadian Sea-ice Biogeochemistry): A sea-ice biogeochemical model for the NEMO community ocean modelling framework. *Geoscientific Model Development* **12**: 1965–1990. DOI: http://dx.doi.org/10.5194/gmd-12-1965-2019.

Hochheim, KP, Barber, DG. 2010. Atmospheric forcing of sea ice in Hudson Bay during the fall period, 1980–2005. *Journal of Geophysical Research* **115**: C05009. DOI: http://dx.doi.org/10.1029/2009JC005334.

Hu, X, Sun, J, Chan, TO, Myers, PG. 2018. Thermodynamic and dynamic ice thickness contributions in the Canadian Arctic Archipelago in NEMO-LIM2 numerical simulations. *The Cryosphere* **12**: 1233–1247.

Ingram, RG, Larouche, P. 1987. Variability of an under-ice river plume in Hudson Bay. *Journal of Geophysical Research* **92**(C9): 9541–9547.

Ingram, RG, Prinsenberg, SJ. 1998. Coastal oceanography of Hudson Bay and surrounding eastern Canadian Arctic waters, in Robinson, AR, Brink, KH eds., *The Sea, vol. 11: The global coastal ocean, regional studies and syntheses*. Chichester, UK: Wiley: 835–861.

Intergovernmental Panel on Climate Change. 2014. Climate change 2014: Synthesis report, in Core writing team, Pachauri, RK, Meyer, LA eds., *Contribution of working groups I, II and III to the fifth assessment report of the intergovernmental panel on climate change*. Geneva, Switzerland: Intergovernmental Panel on Climate Change: 151.

Jafarikhasragh, S, Lukovich, JV, Hu, X, Myers, PG, Sydor, K, Barber, DG. 2019. Modelling sea surface temperature (SST) in the Hudson Bay Complex using bulk heat flux parameterization: Sensitivity to atmospheric forcing and model resolution. *Atmosphere-Ocean* **57**(2): 120–133. DOI: http://dx.doi.org/10.1080/07055900.2019.1605974.

Joly, S, Senneville, S, Caya, D, Saucier, FJ. 2011. Sensitivity of Hudson Bay sea ice and ocean climate to atmospheric temperature forcing. *Climate Dynamics* **36**(9–10): 1835–1849. DOI: http://dx.doi.org/10.1007/s00382-009-0731-4.

Kirillov, S, Babb, D, Dmitrenko, I, Landy, J, Lukovich, J, Ehn, J, Sydor, K, Barber, D, Stroeve, J. 2020. Atmospheric forcing drives the winter sea ice thickness asymmetry of Hudson Bay. *Journal of Geophysical Research: Oceans* **125**(2): e2019JC015756. DOI: http://dx.doi.org/10.1029/2019JC015756.

Landy, JC, Ehn, JK, Babb, DG, Thériault, N, Barber, DG. 2017. Sea ice thickness in the Eastern Canadian Arctic: Hudson Bay Complex and Baffin Bay. *Remote Sensing of Environment* **200**: 281–294.

Lavoie, D, Lambert, N, van der Baaren, A. 2013. Projections of future physical and biogeochemical conditions in Hudson and Baffin Bays from CMIP5 global climate models. Canadian Technical Report of Hydrography and Ocean Sciences, Fisheries and Oceans Canada, Pelagic and Ecosystem Science Branch: 289.

LeBlond, PH, Lazier, JR, Weaver, AJ. 1996. Can regulation of freshwater runoff in Hudson Bay affect the climate of the North Atlantic? *Arctic* **49**(4): 348–355.

Lee, S-Y, Hamlet, AF, Grossman, EE. 2016. Impacts of climate change on regulated streamflow, hydrologic extremes, hydropower production, and sediment discharge in the Skagit River Basin. *Northwest Science* **90**(1): 23–43.

Lilhare, R, Pokorny, S, Déry, SJ, Stadnyk, TA, Koenig, K. 2020. Sensitivity analysis and uncertainty assessment in water budgets simulated by the variable infiltration capacity model for Canadian subarctic watersheds. *Hydrological Processes* **34**(9): 2057–2075.

Lukovich, JV, Barber, DG. 2005. On sea ice concentration anomaly coherence in the Southern Beaufort Sea. *Geophysical Research Letters* **32**(10): L10706.

Macdonald, M, Stadnyk, TA, Dery, SJ, Koenig, K. 2018. Impacts of 1.5°C and 2.0°C warming on pan-Arctic river discharge in the Hudson Bay Complex through 2070. *Geophysical Research Letters* **45**(15): 7561–7570.

Mahlstein, I, Knutti, R. 2012. September Arctic sea ice predicted to disappear near 2°C global warming above present. *Journal of Geophysical Research* **117**: D06104. DOI: http://dx.doi.org/10.1029/2011JD016709.

Morison, J, Kwok, R, Peralta-Ferriz, C, Alkire, M, Rigor, I, Andersen, R, Steele, M. 2012. Changing Arctic Ocean freshwater pathways. *Nature* **481**(7379): 66–70.

Nghiem, SV, Hall, DK, Rigor, IG, Li, P, Neumann, G. 2014. Effects of Mackenzie River discharge and bathymetry on sea ice in the Beaufort Sea. *Geophysical Research Letters* **41**: 873–879.

Notz, D, Stroeve, J. 2016. Observed Arctic sea-ice loss directly follows anthropogenic CO_2 emissions. *Science* **11**: 747–750.

Pokorny, S, Stadnyk, TA, Ali, G, Déry, SJ, Lilhare, R, Koenig, K. 2021. Cumulative effects of uncertainty on simulated streamflow in a hydrologic modelling environment. *Elementa: Science of the Anthropocene* **9**(1): 431. DOI: http://dx.doi.org/10.1525/elementa.431.

Prinsenberg, SJ. 1980. Man-made changes in the freshwater input rates of Hudson and James Bay. *Canadian Journal of Fisheries and Aquatic Sciences* **37**: 1101–1110.

Prinsenberg, SJ. 1983. Effects of the hydroelectric developments on the oceanographic surface parameters of Hudson Bay. *Atmosphere-Ocean* **21**(4): 418–430. DOI: http://dx.doi.org/10.1080/07055900.1983.9649177.

Prinsenberg, SJ. 1991. *Effects of hydro-electric projects on Hudson Bay's marine and ice environments*. Montreal, Canada: North Wind Information Services, Inc. (James Bay Publication series; vol. 2).

Ridenour, NA, Hu, X, Jafarikhasragh, S, Landy, JC, Lukovich, JV, Stadnyk, TA, Sydor, K, Myers, PG, Barber, DG. 2019. Sensitivity of freshwater dynamics to ocean model resolution and river discharge forcing in the Hudson Bay Complex. *Journal of Marine Systems* **196**: 48–64.

Saucier, FJ, Dionne, J. 1998. A 3-D coupled ice-ocean model applied to Hudson Bay, Canada: The seasonal cycle and time-dependent climate response to atmospheric forcing and runoff. *Journal of Geophysical Research* **103**(C12): 27, 689–627, 705.

Saucier, FJ, Senneville, S, Prinsenberg, S, Roy, F, Smith, G, Gachon, P, Caya, D, Laprise, R. 2004. Modelling the sea ice-ocean seasonal cycle in Hudson Bay, Foxe Basin and Hudson Strait, Canada. *Climate Dynamics* **23**: 303–326.

Stadnyk, TA, MacDonald, MK, Tefs, A, Déry, SJ, Koenig, K, Gustafsson, D, Isberg, K, Arheimer, B. 2020. Hydrological modeling of freshwater discharge into Hudson Bay using HYPE. *Elementa: Science of the*

Anthropocene **8**: 43. DOI: http://dx.doi.org/10.1525/elementa.439.

Stadnyk, TA, Tefs, A, Broesky, M, Déry, SJ, Myers, PG, Ridenour, NA, Vonderbank, L, Gustafsson, D. 2021. Changing freshwater contributions to the Arctic: A 90-year trend analysis (1981–2070). *Elementa: Science of the Anthropocene* **9**(1): 00098. DOI: http://dx.doi.org/10.1525/elementa.2020.00098.

Steiner, N, Azetsu-Scott, K, Hamilton, J, Hedges, K, Hu, X, Janjua, MY, Lavoie, D, Loder, J, Melling, H, Merzouk, A, Perrie, W, Peterson, I, Scarratt, M, Sou, T, Tallmann, R. 2015. Observed trends and climate projections affecting marine ecosystems in the Canadian Arctic. *Environmental Reviews* **23**: 191–239.

Stroeve, J, Notz, D. 2015. Insights on past and future sea-ice evolution from combining observations and models. *Global Planetary Change* **135**: 119–132.

Tefs, AAG, Stadnyk, TA, Koenig, KA, Dery, SJ, MacDonald, MK, Slota, P, Crawford, J, Hamilton, M. 2021. Simulating river regulation and reservoir performance in a continental-scale hydrologic model. *Environmental Modelling & Software* **141**. DOI: https://doi.org/10.1016/j.envsoft.2021.105025.

Whittaker, R. 2006. Assessment of the potential environmental impact of the La Grande River Complex on Hudson Bay and the Inuit coastal communities in Northern Québec. GeoArctic – Makivik Report Final Version 1.1, Calgary, Alberta.

How to cite this article: Lukovich, JV, Jafarikhasragh, S, Myers, PG, Ridenour, NA, Castro de la Guardia, LC, Hu, X, Grivault, N, Marson, J, Pennelly, C, Stroeve, JC, Sydor, K, Wong, K, Stadnyk, TA, Barber, DG. 2021. Simulated impacts of relative climate change and river discharge regulation on sea ice and oceanographic conditions in the Hudson Bay Complex. *Elementa: Science of Anthropocene* 9(1). DOI: https://doi.org/10.1525/elementa.2020.00127

Domain Editor-in-Chief: Jody W. Deming, University of Washington, Seattle, WA, USA

Associate Editor: Stephen F. Ackley, Department of Geological Sciences, University of Texas at San Antonio, San Antonio, TX, USA

Knowledge Domain: Ocean Science

Part of an Elementa Special Feature: BaySys

Published: July 16, 2021 **Accepted:** June 20, 2021 **Submitted:** August 29, 2020

ELEMENTA Science of the Anthropocene

Elem Sci Anth is a peer-reviewed open access journal published by University of California Press.

OPEN ACCESS